Raman spectroscopy study of *in situ* change in laser irradiated $LiMn_2O_4$

Zhaojun Liu (刘照军)*, Ligang Han (韩礼刚), and Yujun Mo (莫育俊)

Department of Physics and Electronic Information, Luoyang Normal College, Luoyang 471022, China

**Corresponding author: zhaojunliu@gmail.com*

Received December 16, 2011; accepted March 14, 2012; posted online May 16, 2012

A spinel $LiMn_2O_4$ is investigated via Raman spectroscopy at 514.5-nm excitation and X-ray diffraction. The dependence of Raman spectra on the different irradiated laser powers is determined and found to be different from that at 632.8-nm excitation. Based on our extensive analysis, our experimental results can be attributed to the laser heating effect, which reduces the Mn^{4+} cation concentration in the local area. Consequently, the decrease in average Mn valence in the local area unavoidably induces the Jahn-Teller effect and local lattice distortion, which accounts for the evolution of the measured Raman spectra of spinel $LiMn_2O_4$.

OCIS codes: 300.6450, 290.5860.

doi: 10.3788/COL201210.083001.

Nowadays, lithium ion batteries have dominated the market of small rechargeable batteries mainly because of their harmlessness and high performance[1,2]. Layered oxides $LiMO_2$ (M = Co, Ni) and spinel $LiMn_2O_4$ are the most widely studied cathode materials for lithium ion batteries. Spinel $LiMn_2O_4$ has received a great deal of interest because of its advantages, such as manganese abundance, low cost, easy preparation, and high environmental acceptability[3−7].

Spinel $LiMn_2O_4$ has been studied using many techniques, such as scanning electron microscopy (SEM), atomic force microscopy (AFM), X-ray diffraction (XRD), X-ray photoelectron spectroscopy (XPS), Fourier transform infrared spectroscopy, and differential thermal analysis. Raman spectroscopy has been widely applied in many fields because of its sensitivity and efficacy in detecting different phases and characterizing sample components[8−15]. The Raman modes of spinel $LiMn_2O_4$ have been theoretically studied by some researchers, and the results are consistent[16−18]. However, the measured Raman spectra of $LiMn_2O_4$ differed[12,19−21] in the total amount of Raman bands, band positions, relative intensities, and full-width at half maximum (FWHM) of the corresponding Raman bands. Wei *et al.*[19] prepared the spinel $LiMn_2O_4$ sample using the molten salt method at 700 °C and collected the Raman spectrum on a Renishaw RM-1000 micro-Raman spectrometer at 514.5-nm laser wavelength and 10-mW laser power. Only one broad Raman band at 570–690 cm^{-1} was detected. Prabaharan et al.[20,21] collected the Raman spectrum of spinel $LiMn_2O_4$ on the Jobin-Yvon macro-model U1000 Raman set at 514.5-nm laser wavelength and 10-mW laser power. The Raman spectrum of spinel $LiMn_2O_4$ reported in Ref. [20] was dominated by a strong band at 625 cm^{-1} with a shoulder at 580 cm^{-1}. A medium band appeared at 482 cm^{-1} together with three weak bands at 370, 298, and 204 cm^{-1}. However, in the results in Ref. [21], the three weak bands appeared at approximately 426, 382, and 300 cm^{-1}. The different sample preparation methods may be one possible reason for the difference. The former spinel $LiMn_2O_4$ was prepared via soft-chemistry synthesis at 250 °C, whereas the latter was prepared via solid-state reaction at 750 °C.

Paolone *et al.*[12] studied the dependence of the Raman spectrum of spinel $LiMn_2O_4$ on the excitation laser power. They concluded that the spinel $LiMn_2O_4$ in the irradiated area by higher laser power transformed into Mn_3O_4 because of laser-induced thermal decomposition. In addition, they believed that the original Raman spectrum of $LiMn_2O_4$ consisted of a broad band at 580 cm^{-1} and two additional poorly defined modes between 300 and 400 cm^{-1}. Their sample was synthesized via the solid-state method at 800 °C, and the Raman spectra were recorded on a LabRam micro-Raman spectrometer with an excitation laser of 632.8 nm. The results obtained by previous researchers are complex and controversial. Thus, a further study is necessary to deepen the understanding of the Raman spectrum of spinel $LiMn_2O_4$.

In this letter, the Raman spectra of spinel $LiMn_2O_4$ were obtained at different laser powers. The Raman bands were assigned based on the theoretical results[17,18]. The corresponding band position, relative intensity, and FWHM parameters were analyzed and compared. The evolution of the Raman spectra was attributed to the reduction of the Mn^{4+} cation concentration and local lattice distortion induced by the Jahn-Teller effect.

The spinel $LiMn_2O_4$ (Nippon Chemicals, battery grade) cathode material and Mn_3O_4 (Shanghai No. 1 Chemical Reagent Factory) were used as provided (both polycrystalline powder). The XRD pattern of the sample was collected on a Holland X'Pert Pro MPD X-ray diffractometer equipped with monochromatized Cu-Kα radiation ($\lambda = 0.15418$ nm). The diffraction pattern was taken in the 2θ range ($10° \leqslant 2\theta \leqslant 90°$) at room temperature.

The Raman spectra were obtained in air with a Jobin-Yvon HR800 microspectrophotometer equipped with a CCD detector. The 514.5-nm line of Spectra-Physics 163C air-cooled Ar^+ laser was chosen as the excitation source. A 50× objective was used to perform a 180° backward scattering configuration, and the diameter of the pinhole was 300 μm. Thus, a laser spot of approximately 2 μm in diameter was obtained on the sample.

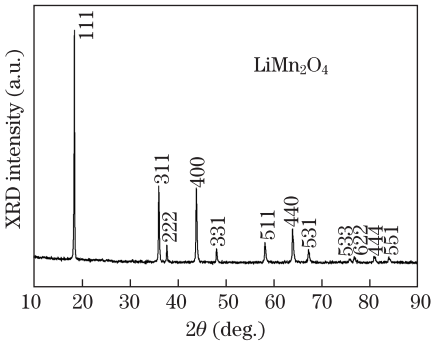

Fig. 1. XRD pattern of spinel $LiMn_2O_4$ powder.

The spectral resolution was about 2 cm^{-1} with a 1800 groove/mm grating monochromator.

The full laser power on the sample was about 2 mW, and the laser power stability was ±1%. A set of neutral density filters was introduced to reduce the laser power on the sample. The filters can reduce the laser power to 1%, 10%, 25%, 50%, and 100% of the full laser power, respectively. The Raman spectra of spinel $LiMn_2O_4$ were collected starting from the highest filter and so on by increasing the laser power on the sample (i.e., from 1% to 100%). The acquisition time of each spectrum varied from 10 s (100% laser power) to 600 s (1% laser power), and three acquisitions were averaged to obtain a reasonable signal-to-noise ratio (SNR).

The XRD pattern of the spinel $LiMn_2O_4$ is shown in Fig. 1. All diffraction peaks can be indexed to the cubic lattice ($Fd\bar{3}$m space group) with $a = 0.8236$ nm. The results confirm the formation of the spinel structure without any detected impurity phases, indicating that the quality of the sample is good enough for this study.

The cubic spinel $LiMn_2O_4$ possesses O_h^7 symmetry, where the lithium ions occupy the tetrahedral 8a sites, the manganese cations reside on the octahedral 16d sites, and the oxygen anions are on the 32e sites. Based on the group theory analysis of O_h^7 symmetry, the MnO_6 octahedron yields five Raman active vibrational modes (A_{1g}+E_g+$3F_{2g}$), of which A_{1g} stands for the symmetric stretching mode, E_g for the symmetric deformation mode, and F_{2g} for the symmetric bending mode[22,23].

Figure 2 shows the Raman spectra of spinel $LiMn_2O_4$ and Mn_3O_4 at a relatively low laser power (0.5 mW on sample). The Raman spectrum of $LiMn_2O_4$ is dominated by a strong band at 626 cm^{-1} with a weak shoulder at 584 cm^{-1}, and three weak bands at 479, 382, and 298 cm^{-1}. This experimental result is similar to those in Refs. [20,24] and consistent with theoretical results[17,18]. These results are compared in Table 1. The band at 626 cm^{-1} can be assigned to the symmetric Mn-O stretching vibration of the MnO_6 groups for the A_{1g} symmetry in the O_h^7 space group[20,21]. Its broadening may be attributed to the slightly different structures between the isotropic $Mn^{4+}O_6$ octahedra and the locally distorted $Mn^{3+}O_6$ octahedra in spinel $LiMn_2O_4$[19,21]. The shoulder at 584 cm^{-1} can be assigned to the $F_{2g}^{(1)}$ mode originating from the symmetric bending vibration of the Mn-O bond. Its intensity depends on the Mn^{4+} concentration in the material and reflects the Mn average oxidation state[19,21]. The weak band at 382 cm^{-1} has E_g symmetry, and the other two weak bands at 479 and 298 cm^{-1} are assigned to the $F_{2g}^{(2)}$ and $F_{2g}^{(3)}$ modes, respectively. Here, the Raman spectrum of Mn_3O_4 is also given (Fig. 2) as reference.

Figure 3 demonstrates the Raman spectra of spinel $LiMn_2O_4$ at different laser powers. No new Raman band can be found except those of spinel $LiMn_2O_4$, indicating that the local component of the sample does not change as the laser powder increases. The decomposition of $LiMn_2O_4$ and generation of Mn_3O_4 did not occur in our experiment. However, the parameters (such as the position, relative intensities, and FWHW) of Raman bands assigned to $LiMn_2O_4$ changed significantly. The difference between our experimental results and those of Ref. [12] may be due to the following three reasons. Firstly, samples prepared by different methods may have different microstructures and properties, which unavoidably affect the Raman spectra of samples. Secondly, different excitation laser wavelengths may result in slight variations in Raman spectra. Finally, the laser power in this study, which is different from that in Ref. [12], reduces the Mn^{4+} concentration in the material instead of the chemical decomposition because of the increase in the local temperature of the measured area. The decomposition of $LiMn_2O_4$ would not occur until the laser power reached a critical value.

Close inspection of the spectra in Fig. 3 shows a gradual evolution in band position, relative intensity, and FWHM, whose variations are plotted in Fig. 4. First, we fitted the spectrum at 100% laser power using mixed Lorentzian and Gaussian profiles. Then, the optimal fitting ratio (69.2% Lorentzian for A_{1g} mode and 47.6% Lorentzian for $F_{2g}^{(1)}$ mode) was selected to deal with the other spectra. The measured Raman intensity strongly depends on the laser power. Thus, the ratio of the

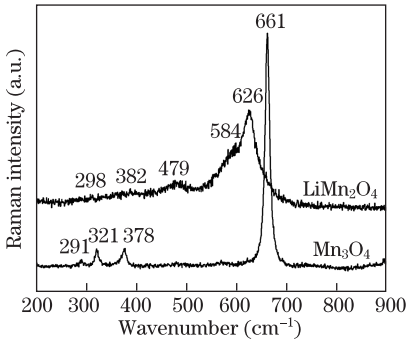

Fig. 2. Raman spectra of spinel $LiMn_2O_4$ and Mn_3O_4 at 0.5-mW laser power.

Table 1. Experimental Raman Frequencies of the Spinel $LiMn_2O_4$ Compared with Theoretical Values

Mode	Frequency (cm^{-1})			
	Present Experiments		Calculated[17]	Calculated[18]
A_{1g}	626		625	598
E_g	382		432	434
$F_{2g}^{(1)}$	584		618	597
$F_{2g}^{(2)}$	479		543	455
$F_{2g}^{(3)}$	298		337	354

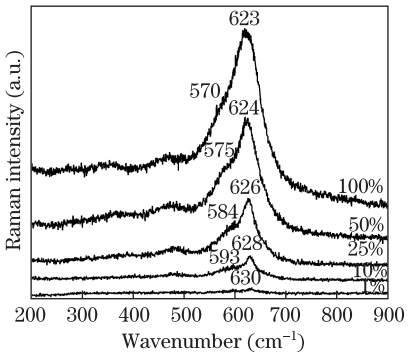

Fig. 3. Raman spectra of spinel $LiMn_2O_4$ at different laser powers.

integral intensity of the $F_{2g}^{(1)}$ mode and the corresponding A_{1g} mode of each Raman spectrum was calculated to reflect the intrinsic change of the sample with the fitting method mentioned before. Figure 4(a) shows that the ratio of the integral intensity of the $F_{2g}^{(1)}$ mode and the corresponding A_{1g} mode of each spectrum distinctly reduces as laser power increases. The $F_{2g}^{(1)}$ mode has been known to originate from the symmetric bending vibration of Mn^{4+}-O, and the A_{1g} mode stands from the Mn-O symmetric stretching vibration[19,21]. Thus, the Mn^{4+} concentration decreased as laser power increased. The Jahn-Teller distortion is substantially caused by the cooperative interaction of the local distortions around Mn^{3+} ions, which are in octahedral sites. The tetragonal distortion c/a exists between $2.2 \leqslant x \leqslant 3.5$ in Mn^{x+} with the maximum at $x = 3.0$[25]. The average valence of Mn in spinel $LiMn_2O_4$ is 3.5. Hence, even a slight external perturbation can induce Jahn-Teller distortion. Laser heating can also be regarded as an external perturbation because the increase in laser power increases the local area temperature of the measured sample[26]. Moreover, $LiMn_2O_4$ is a small-polaron semiconductor, in which electron hopping occurs between Mn^{3+} and Mn^{4+} in the material[27]. The increase in local temperature caused by the laser heating effect accelerates the motion of carriers and the charge carrier migration ($Mn^{4+} \rightarrow Mn^{3+}$) in the material. Hence, the laser-heating effect ultimately causes the increase in Mn^{3+} concentration and decrease in Mn^{4+} concentration in the area involved in the Raman

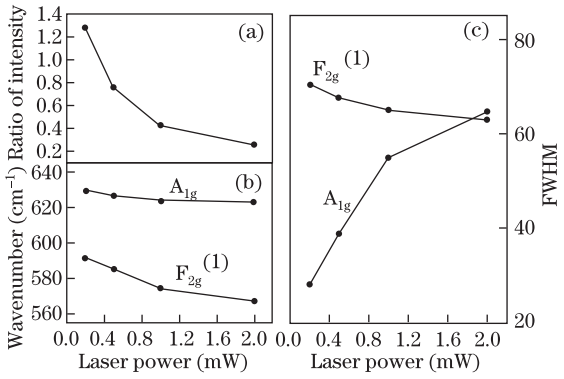

Fig. 4. Dependence of the (a) ratio of integral intensity of $F_{2g}^{(1)}/A_{1g}$, (b) peak position, and (c) FWHM of the A_{1g} mode around 625 cm^{-1} and $F_{2g}^{(1)}$ mode around 580 cm^{-1} on laser power.

measurements. This phenomenon decreases the average valence of Mn in the local area, leading to the Jahn-Teller distortion.

Generally, as the temperature increases, all the Raman bands tend to show both an overall broadening and a shift to lower frequencies. Figure 4(b) shows that both the A_{1g} and $F_{2g}^{(1)}$ Raman modes have red shifted as laser power increased. However, this shift could not be attributed to the increase in local temperature induced by laser heating because it could not explain the broadening of the A_{1g} mode and narrowing of the $F_{2g}^{(1)}$ mode in Fig. 4(c). Therefore, the red shift (Fig. 4(b)) and the variation of FWHM (Fig. 4(c)) cannot be simply explained by the local temperature increase induced by the laser-heating effect. However, it should be attributed to the local lattice distortion derived from the Jahn-Teller effect.

In conclusion, based on our Raman spectroscopy study of spinel $LiMn_2O_4$, laser irradiation reduces the Mn^{4+} cation concentration in the material. Moreover, the relative intensity of the $F_{2g}^{(1)}$ mode decreases with the decrease in Mn^{4+} cation concentration in the material. The decrease in the Mn^{4+} cation concentration accompanied by the decrease in the average valence of Mn in the local area induces the Jahn-Teller effect. The local lattice distortion derived from the Jahn-Teller effect varies the Raman band parameters.

This work was supported by the National Natural Science Foundation of China under Grant No. 10674041.

References

1. K. Ozawa, Solid State Ionics **69,** 212 (1994).
2. T. Nagaura and K. Tazawa, Progress in Batteries and Solar Cells **9,** 209 (1990).
3. T. Ohzuku, M. Kitagawa, and T. Hirai, J. Electrochem. Soc. **137,** 769 (1990).
4. S. Magahed and B. Scrosati, J. Power Sources **51,** 79 (1994).
5. M. M. Thackeray, Prog. Solid. St. Chem. **25,** 1 (1997).
6. Y. Xia, H. Takeshige, H. Noguchi, and M. Yoshio, J. Power Sources **56,** 61 (1995).
7. J. M. Tarascon, E. Wang, F. K. Sholooki, W. R. Mckinnon, and S. Colson, J. Electrochem. Soc. **138,** 2859 (1991).
8. Y. Bai, Y. Lan, and Y. Mo, Acta Phys. Sin. (in Chinese) **54,** 4654 (2005).
9. X. Liu, C. Huang, J. Qiu, and Y. Wang, Appl. Surf. Sci. **253,** 2747 (2006).
10. S. J. Rigby, A. H. R. Al-Obaidi, S. K. Lee, D. McStay, and P. K. J. Robertson, Appl. Surf. Sci. **252,** 7948 (2006).
11. S.W. Song, K. S. Han, H. Fujita, and M. Yoshimura, Chem. Phys. Lett. **344,** 299 (2001).
12. A. Paolone, A. Sacchetti, T. Corridoni, P. Postorino, R. Cantelli, G. Rousse, and C. Masquelier, Solid State Ionics **170,** 135 (2004).
13. H. Zhao, H. Cheng, Q. Li, and F. Gan, Chin. Opt. Lett. **9,** 033001 (2011).
14. E. Tan, P. Yin, L. Li, and L. Guo, Chin. Opt. Lett. **9,** 082901 (2011).
15. Y. Bai, Y. Lan, H. Zhu, and Y. Mo, Acta Opt. Sin. (in Chinese) **25,** 1712 (2005).

16. W. B. White and B. A. DeAngelis, Spectrochim. Acta **23A,** 985 (1967).
17. M. M. Sinha and H. C. Gupta, Phys. B **316,** 166 (2002).
18. B. Ammudsen, G. R. Burns, M. S. Islam, H. Kanoh, and J. Roziere, J. Phys. Chem. B **103,** 5175 (1999).
19. Y. Wei, K. W. Nam, K. B. Kim, and G. Chen, Solid State Ionics **177,** 29 (2006).
20. S. R. S. Prabaharan, N. B. Saparil, S. S Michael, M. Massot, and C. M. Julien, Solid State Ionics **112,** 25 (1998).
21. C. M. Julien and M. Massot, Mater. Sci. Eng. B **97,** 217 (2003).
22. G. C. Allen and M. Paul, Appl. Spectrosc. **49,** 451 (1995).
23. G. A. Nazri and C. Jullien, Ionics **2,** 1 (1996).
24. S. R. S. Prabaharan, S. S. Michael, and C. M. Jullien, Int. J. Inorg. Mater. **1,** 21 (1999).
25. A. Yamada and M. Tanaka, Mater. Res. Bull. **30,** 715 (1995).
26. A. Paolone, P. Roy, G. Rousse, C. Masqnelier, and J. Rodriguez-Carvajal, Solid State Commun. **111,** 453 (1999).
27. J. B. Goodenough, A. Manthiram, and B. Wnetrzewski, J. Power Sources **43,** 269 (1993).